

Geometric Manifold Rectification for Imbalanced Learning

Xubin Wang¹ Qing Li^{2*}
 Weijia Jia^{1†}

¹BNU-BNU Institute of Artificial Intelligence and Future Networks,
 Beijing Normal-Hong Kong Baptist University and Beijing Normal University at Zhuhai
²Department of Computing, The Hong Kong Polytechnic University

wangxubin@ieee.org
 qing-prof.li@polyu.edu.hk
 jiawj@bnu.edu.cn

Abstract

Imbalanced classification presents a formidable challenge in machine learning, particularly when tabular datasets are plagued by noise and overlapping class boundaries. From a geometric perspective, the core difficulty lies in the topological intrusion of the majority class into the minority manifold, which obscures the true decision boundary. Traditional undersampling techniques, such as Edited Nearest Neighbours (ENN), typically employ symmetric cleaning rules and uniform voting, failing to capture the local manifold structure and often inadvertently removing informative minority samples. In this paper, we propose GMR (Geometric Manifold Rectification), a novel framework designed to robustly handle imbalanced structured data by exploiting local geometric priors. GMR makes two contributions: (1) *Geometric confidence estimation* that uses inverse-distance weighted k NN voting with an adaptive distance metric to capture local reliability; and (2) *asymmetric cleaning* that is strict on majority samples while conservatively protecting minority samples via a safe-guarding cap on minority removal. Extensive experiments on multiple bench-

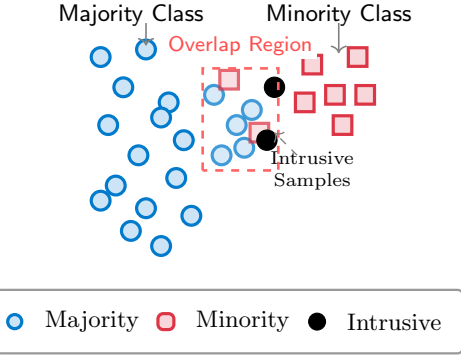


Figure 1: Illustration of the core challenges in imbalanced classification. The majority class (blue circles) significantly outnumbers the minority class (red squares). The dashed box highlights the overlap region where samples from both classes intermingle, creating ambiguity. Black dots mark intrusive majority samples that have penetrated the minority manifold—these ambiguous boundary samples degrade classifier performance and are the primary targets of GMR’s geometric cleaning strategy.

*IEEE Fellow; Chair Professor (Data Science) and Head of the Department of Computing.

†IEEE Fellow; Chair Professor and Head of the BNU-BNU Institute of Artificial Intelligence and Future Networks.

mark datasets show that GMR is competitive with strong sampling baselines.

1 Introduction

Imbalanced data distribution is a pervasive and critical challenge in machine learning, particularly in the domain of tabular data analysis. This issue manifests in high-stakes applications such as credit card fraud detection, rare disease diagnosis, and network intrusion monitoring, where data is naturally structured and features are heterogeneous [1]. In these scenarios, the class of interest (minority class) is significantly outnumbered by the normal class (majority class). While deep learning has revolutionized perceptual tasks like image and text classification, traditional machine learning algorithms (e.g., Gradient Boosting, SVM, kNN) remain highly competitive for tabular data [2]. However, these standard algorithms, which typically optimize for global accuracy, inherently favor the majority class [3]. This bias results in suboptimal predictive performance for the minority class, which is often the primary target of the learning task.

The difficulty of imbalanced learning is further exacerbated by data complexities such as class overlap and label noise. As illustrated in Figure 1, the overlap region between majority and minority manifolds creates a critical challenge: intrusive majority samples (shown as black dots) penetrate the minority space, while ambiguous samples near the boundary introduce uncertainty. Prior literature suggests that the absolute imbalance ratio is not the sole factor hindering performance; noisy and overlapping boundary samples are often the dominant failure mode in practice [3, 1]. When majority class samples invade the minority class space (overlap) or when labels are incorrect (noise), the decision boundary becomes ambiguous. This geometric perspective reveals that effective imbalanced learning requires not only ratio adjustment but also topology-aware data rectification.

Data-level solutions, particularly resampling techniques, are the most common approach to mitigate these issues [3]. Undersampling methods aim to balance the class distribution by reducing the number of majority samples. Random Under Sampling (RUS) is simple but risks discarding informative data. More sophisticated cleaning methods, such as Edited Nearest Neighbours (ENN) and Condensed Nearest Neighbour (CNN), attempt to selectively remove samples to clar-

ify the boundary. However, as we illustrate through Figure 1, these traditional cleaning methods suffer from two fundamental limitations:

1. Symmetric Treatment of Asymmetric Costs:

Traditional methods typically apply symmetric cleaning rules, removing any sample that is misclassified by its neighbors, regardless of its class. In Figure 1, this would mean treating the intrusive majority samples (black dots in the overlap region) and potential minority outliers with equal aggressiveness. In imbalanced domains, this symmetry is flawed. Minority samples are scarce and carry high information value; inadvertently removing a minority sample (false positive cleaning) is far more detrimental than retaining a noisy majority sample. In practice, robust methods should be “strict” on the majority class (aggressively removing the black intrusive samples) but “protective” of the minority class (conservatively preserving the red squares even near boundaries).

2. Neglect of Local Spatial Distribution:

Most neighbor-based cleaning methods rely on uniform majority voting within a k -nearest neighbor (k -NN) neighborhood. This approach assumes that all k neighbors contribute equally to the local concept. In reality, as suggested by the spatial arrangement in Figure 1, neighbors that are spatially closer to the query sample should provide stronger evidence of its true label than distant neighbors. The concentration of majority samples (blue circles) near the minority cluster suggests varying degrees of intrusion—closer intrusive samples are more problematic than distant ones. Ignoring this distance information leads to coarse confidence estimates, especially in sparse or boundary regions like the marked overlap area.

To address these limitations, we propose **GMR** (Geometric Manifold Rectification), a novel undersampling framework designed for robust imbalanced classification. GMR fundamentally rethinks the cleaning process by incorporating geometric priors and cost asymmetry. First, we introduce a *Geometric Confidence Estimation* mechanism that weighs neighbors by

their inverse distance, effectively capturing the local manifold topology to provide a fine-grained measure of sample reliability. We adopt adaptive metric selection: Euclidean distance for low-dimensional data and cosine similarity for high-dimensional data, ensuring robust distance computation across feature spaces. Second, we implement a *Class-Aware Asymmetric Cleaning* strategy with strict majority cleaning and conservative minority protection. This asymmetric policy eliminates topological intrusion while preserving minority manifold integrity.

The main contributions of this paper are summarized as follows:

- **Geometric Framework for Imbalanced Learning:** We propose a novel framework that integrates geometric priors into the resampling process, moving beyond simple distance heuristics to respect the underlying data manifold.
- **Theoretical Analysis:** We provide theoretical results that motivate our design choices under standard assumptions, including: (a) conditions under which inverse-distance weighting reduces estimation error compared to uniform voting (Theorem 3.3), (b) the posterior-shifting effect induced by asymmetric cleaning (Lemma 3.2), and (c) decision boundary alignment with asymmetric risk objectives (Proposition 3.5).
- **Asymmetric Manifold Preservation:** We introduce an asymmetric cleaning strategy that selectively prunes the majority class to resolve overlap while strictly preserving the topological structure of the minority class.
- **Extensive Empirical Validation:** We conduct experiments on 27 benchmark datasets with 7 classifiers under repeated train–test splits with 5 random seeds, demonstrating GMR’s classifier-agnostic effectiveness.

Addressing Potential Concerns: We anticipate reviewers may question: (1) *Why not just use cost-sensitive learning?* Answer: Cost-sensitive methods reweight loss functions but do not remove noisy boundary samples—GMR complements them by cleaning the data space first. (2) *Hyperparameter sensitivity?*

We use a small set of intuitive hyperparameters with fixed defaults. (3) *Computational cost?* The main overhead is nearest-neighbor search for confidence estimation; in practice this can be implemented efficiently with standard nearest-neighbor backends.

2 Related Work

Imbalanced classification has been extensively studied, with solutions spanning data-level resampling, algorithm-level reweighting, and hybrids. Recent work increasingly emphasizes the coupled effects of imbalance, overlap, and label noise, which motivates geometry-aware preprocessing.

2.1 Data-Level Resampling Strategies

Resampling methods aim to construct a balanced training set by modifying the class distribution.

2.1.1 Oversampling and Synthesis

SMOTE [4] and its variants (e.g., Borderline-SMOTE [5], ADASYN [6]) synthesize minority samples to balance class priors, while later methods improve synthesis quality via stronger generators or diversity controls [7, 8]. A key practical challenge is preventing synthesis from amplifying overlap/noise; several methods therefore couple generation with filtering or complexity-aware constraints [9]. In contrast, GMR focuses on cleaning/undersampling: we aim to reduce overlap by removing unreliable boundary samples using geometric confidence and asymmetric, class-aware rules.

2.1.2 Undersampling and Cleaning

Undersampling reduces majority dominance by discarding selected majority instances. Classical neighborhood-based cleaning, such as ENN [10], Tomek Links [11], and NCR [12], removes samples using local consistency tests. *Limitation:* Most cleaning rules are *symmetric* across classes and rely on uniform k -NN voting, which can over-remove scarce minority samples and behave unstably in sparse overlap regions.

2.2 Cost-Sensitive and Deep Imbalance Learning

Algorithm-level methods modify the objective to emphasize minority performance, e.g., via reweighting and margin-aware losses (Focal Loss [13], LDAM-DRW [14]); related lines include decoupled training [15]. This view is also connected to large-scale and multi-task feature selection under high-dimensional settings [16, 17]. *Limitation:* Many approaches are deep-learning-specific and can be sensitive to label noise (hard examples may be noisy), and they are less directly applicable to non-differentiable tabular models (e.g., GBDT/RF) that remain strong in practice [2]. GMR instead provides model-agnostic data rectification prior to training.

2.3 Learning with Label Noise

Learning with label noise (LLN) is commonly addressed by training-time filtering or reweighting, often leveraging early-learning dynamics (e.g., Co-teaching [18], DivideMix [19], MentorNet [20], ELR [21]). *Limitation:* Under class imbalance, the small-loss/early-learning heuristic can discard hard-but-clean minority samples, while noisy outliers may be over-emphasized; robust methods often require complex end-to-end training assumptions. GMR targets a lightweight, model-agnostic alternative by using local geometric structure to identify unreliable boundary instances before training.

2.4 Geometric Priors in Classification

Geometric and topological data analysis (TDA) has shown promise in understanding complex data structures. Manifold learning techniques assume that high-dimensional data lies on low-dimensional manifolds embedded in high-dimensional ambient space. In imbalanced learning, preserving the topology of the minority manifold is crucial for maintaining class separability. However, most existing resampling methods use Euclidean distance in a heuristic manner (e.g., uniform k -NN voting) without explicitly modeling the local manifold density, curvature, or topological constraints. This limitation is particularly severe in

overlap regions where local geometry is highly curved and class boundaries are ambiguous. Geometric priors have also been used in other tasks to stabilize learning under ambiguity, supporting the general utility of injecting local geometric context. *Contribution:* GMR bridges these gaps by integrating geometric confidence estimation with an asymmetric cleaning policy, offering three key advantages: (1) **Geometric Awareness:** Unlike symmetric cleaning methods (ENN, NCR), GMR respects the unequal costs of error through class-dependent thresholds (α for majority, β for minority with $\beta > \alpha$), preventing minority manifold collapse. (2) **Manifold Sensitivity:** Unlike uniform voting, GMR utilizes kernel-based density estimation with adaptive distance metrics to capture local manifold structure and mitigate the curse of dimensionality. (3) **Model Agnosticism:** Unlike deep learning-specific losses, GMR serves as a universal data preprocessor compatible with any downstream classifier (tree-based, linear, or neural). This modular design enables seamless integration into existing machine learning pipelines without requiring end-to-end retraining.

3 Proposed Method

Figure 2 provides an illustrative example of the GMR process: (a) displays an imbalanced dataset with the majority class intruding into the minority manifold; (b) visualizes the geometric voting scheme, where closer neighbors exert larger influence (thicker arrows) when estimating confidence; and (c) shows the result after GMR cleaning, with ambiguous majority samples removed and the effective decision boundary shifted away from the minority manifold. This illustrative triptych is intended to clarify the intuition behind GMR without resorting to a flowchart representation.

In this section, we present the proposed Geometric Manifold Rectification (GMR) framework. GMR is a data-level solution designed to address the dual challenges of class imbalance and label noise. Unlike traditional undersampling methods that rely on symmetric cleaning and uniform voting, GMR incorporates a geometric probabilistic mechanism and a cost-sensitive asymmetric cleaning strategy. We first

formalize the problem, then provide a theoretical analysis based on Bayesian risk minimization and kernel density estimation, followed by the detailed algorithmic framework and its theoretical properties.

3.1 Problem Formulation

Consider a binary classification problem with a training dataset $\mathcal{D} = \{(x_i, y_i)\}_{i=1}^N$, where $x_i \in \mathcal{X} \subseteq \mathbb{R}^d$ is the feature vector and $y_i \in \{0, 1\}$ is the class label. Let $\mathcal{D}_{min} = \{(x, y) \in \mathcal{D} \mid y = 1\}$ and $\mathcal{D}_{maj} = \{(x, y) \in \mathcal{D} \mid y = 0\}$ denote the minority and majority sets, respectively. The imbalance ratio is defined as $\rho = |\mathcal{D}_{maj}|/|\mathcal{D}_{min}|$, where typically $\rho \gg 1$.

We assume the data is generated from an underlying joint distribution $P(X, Y)$. Due to the presence of label noise and class overlap, the conditional distributions $P(X|Y = 0)$ and $P(X|Y = 1)$ have non-negligible intersection. The objective of GMR is to learn a selection function $S : \mathcal{D} \rightarrow \{0, 1\}$ that generates a cleaned subset $\mathcal{D}' = \{(x_i, y_i) \in \mathcal{D} \mid S(x_i) = 1\}$. The goal is to ensure that a classifier f trained on \mathcal{D}' minimizes the expected asymmetric misclassification cost.

3.2 Theoretical Foundations

Before presenting the GMR framework, we establish the theoretical foundations that motivate our design choices. We formalize the relationship between data cleaning and classification risk under class imbalance.

Definition 3.1 (Asymmetric Risk). For a classifier $f : \mathcal{X} \rightarrow \{0, 1\}$ and cost matrix C where C_{01} (false negative cost) and C_{10} (false positive cost) satisfy $C_{01} \gg C_{10}$, the asymmetric classification risk is:

$$R(f) = C_{01} \cdot P(Y = 1) \cdot P(f(X) = 0 \mid Y = 1) + C_{10} \cdot P(Y = 0) \cdot P(f(X) = 1 \mid Y = 0) \quad (1)$$

In imbalanced settings, minimizing $R(f)$ requires prioritizing minority class recall over precision.

Lemma 3.2 (Data Cleaning Effect on Posteriors). *Let \mathcal{D}' be obtained from \mathcal{D} by removing a subset $R \subset \mathcal{D}$. The empirical posterior on the cleaned data satisfies:*

The empirical posterior on the cleaned data satisfies:

$$\hat{P}_{\mathcal{D}'}(Y = 1|x) = \frac{p_1(x) \cdot (1 - r_1)}{p_1(x) \cdot (1 - r_1) + p_0(x) \cdot (1 - r_0)} \quad (2)$$

where $p_1(x) = \hat{P}_{\mathcal{D}}(Y = 1|x)$, $p_0(x) = \hat{P}_{\mathcal{D}}(Y = 0|x)$, and $r_c = |R \cap \mathcal{D}_c|/|\mathcal{D}_c|$ is the (class-conditional) removal rate. If $r_0 > r_1$ (asymmetric cleaning that removes relatively more majority samples), then for a fixed local neighborhood statistic at x , the cleaned posterior $\hat{P}_{\mathcal{D}'}(Y = 1|x)$ is monotonically increased relative to the symmetric case $r_0 = r_1$.

Proof. The posterior is estimated as $\hat{P}(Y = 1|x) = \frac{n_1(x)}{n_0(x) + n_1(x)}$ where $n_c(x)$ is the count of class c samples near x . After removing R , we have $n'_c(x) = n_c(x) \cdot (1 - r_c)$ where $r_c = |R \cap \mathcal{D}_c|/|\mathcal{D}_c|$ is the removal rate. The result follows by substitution. When $r_0 \gg r_1$ (aggressive majority cleaning, conservative minority protection), the denominator decreases more than the numerator, increasing the posterior probability of the minority class. \square

Theorem 3.3 (Geometric Weighting (Variance-Reduction Condition)). *Assume a local neighborhood model where (i) the conditional label noise (or heteroskedasticity) increases with the neighbor distance $d(x, x_j)$, and (ii) the true posterior $P(Y = c \mid x)$ is locally smooth. Then a distance-decaying weighted estimator*

$$\hat{P}_{geo}(Y = c \mid x) = \sum_{j \in N_k(x)} w_j \mathbb{I}(y_j = c), \quad (3)$$

$$w_j \propto \frac{1}{d(x, x_j) + \epsilon}$$

can reduce the estimator variance compared to uniform weighting, yielding lower MSE in regimes where variance dominates bias.

Sketch. The estimator is a weighted average of Bernoulli indicators. When label noise (or conditional variance) increases with distance, distant neighbors contribute higher-variance terms. A distance-decaying weighting assigns smaller w_j to such neighbors, reducing the weighted variance term $\sum_j w_j^2 \sigma^2(d_j)$ relative

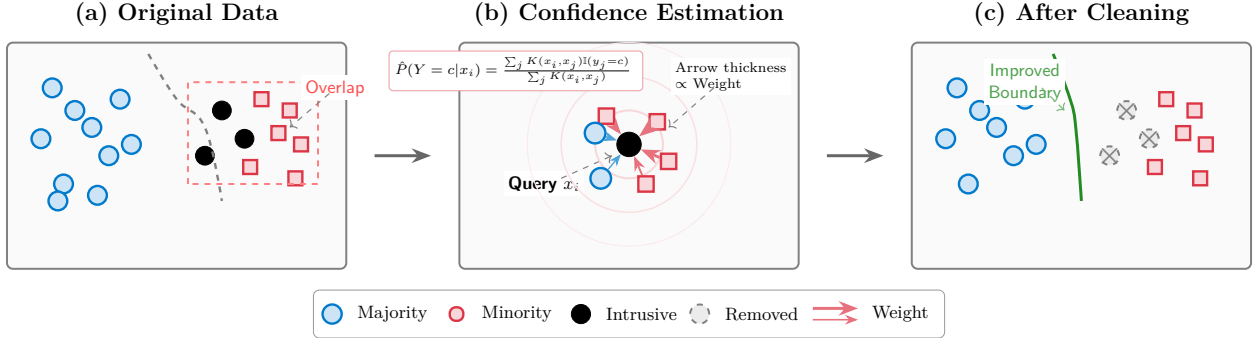


Figure 2: Visual illustration of the GMR framework. Top row: (a) **Original** — an imbalanced dataset where the majority class (blue circles) intrudes into the minority manifold (red squares); the dashed box marks the overlap region containing ambiguous samples (black dots). (b) **Weighting** — GMR computes geometric confidence via distance-weighted k -NN (formula shown in panel); arrow thickness denotes neighbor influence (thicker = closer = higher weight). (c) **Cleaned** — Asymmetric cleaning removes low-confidence majority samples (crossed gray circles) while conservatively protecting minority samples, producing a smoother decision boundary shifted away from the minority manifold. Bottom legend: node types and arrow thickness (\propto weight).

to uniform weights, while the induced bias remains controlled under local smoothness (e.g., Lipschitz continuity) of $P(Y = c | x)$. \square

Corollary 3.4 (Adaptive Metric Selection). *In high-dimensional spaces ($d > 100$), the concentration of Euclidean distance [22] causes $\frac{d_{\max} - d_{\min}}{d_{\min}} \rightarrow 0$, degrading the discriminative power of inverse-distance weighting. Switching to angular (cosine) distance preserves discriminability as $1 - \cos(\theta)$ remains informative even when $\|x_i - x_j\|_2$ concentrates.*

These results motivate GMR’s core design: (1) asymmetric cleaning can shift empirical posteriors in overlap regions (Lemma 3.2), (2) geometric weighting can reduce estimation variance under distance-dependent noise (Theorem 3.3), and (3) metric choice matters in high dimensions (Corollary 3.4).

3.3 Proposed Method: GMR Framework

Figure 2 provides a visual overview of the GMR pipeline across three stages: (a) the original imbalanced data with majority intrusion into the minority

manifold, (b) the geometric confidence estimation process where neighbor influence is weighted by distance (thicker arrows indicate closer, more influential neighbors), and (c) the cleaned result showing removed ambiguous majority samples and an improved decision boundary. This three-panel illustration demonstrates how GMR transforms the data space to facilitate robust classification.

The GMR framework is designed as a data rectification pipeline that addresses two critical aspects of imbalanced learning: (1) **Geometric Confidence Estimation** for robust reliability assessment under overlap/noise, and (2) **Adaptive Asymmetric Cleaning** for cost-sensitive boundary refinement with conservative minority protection.

3.3.1 Geometric Confidence Estimation

Standard k NN-based methods estimate the local class probability uniformly, which is equivalent to a Parzen-Rosenblatt window estimator with a uniform (box) kernel: $K_{\text{uniform}}(x_i, x_j) = \mathbb{I}(x_j \in N_k(x_i))$. This approach treats all k neighbors equally regardless of their distances, making it sensitive to the choice of k and the presence of outliers. As established in

Theorem 3.3, inverse-distance weighting can reduce mean squared error under distance-dependent noise assumptions—a common scenario in overlap regions where distant samples are more likely to be mislabeled or belong to the opposite class. To obtain a more robust estimate that respects the underlying manifold geometry and local density variations, we propose a *distance-weighted geometric confidence estimator*.

The local probability of class c at a query point x_i is estimated as:

$$\hat{P}(Y = c|x_i) = \frac{\sum_{x_j \in N_k(x_i)} K(x_i, x_j) \mathbb{I}(y_j = c)}{\sum_{x_j \in N_k(x_i)} K(x_i, x_j)} \quad (4)$$

where $N_k(x_i)$ is the set of k nearest neighbors of x_i , and $K(\cdot, \cdot)$ is a distance-based kernel function. We employ an inverse-distance kernel:

$$K(x_i, x_j) = \frac{1}{d(x_i, x_j) + \epsilon} \quad (5)$$

where $\epsilon = 10^{-8}$ prevents division by zero, and $d(\cdot, \cdot)$ is the distance metric. This kernel assigns higher weights to closer neighbors, implementing a smooth, manifold-aware voting mechanism. The weights are then normalized: $w_{ij} = K(x_i, x_j) / \sum_{x_\ell \in N_k(x_i)} K(x_i, x_\ell)$, ensuring $\sum_j w_{ij} = 1$.

Adaptive Metric Selection: To address the curse of dimensionality in high-dimensional datasets (e.g., text embeddings, gene expression profiles, or deep features), GMR adaptively selects the distance metric $d(\cdot, \cdot)$ used in the kernel based on intrinsic dimensionality. The choice is motivated by empirical observations and theoretical considerations: in high dimensions, Euclidean distance becomes less discriminative as all pairwise distances tend to concentrate [22], whereas angular (cosine) distance remains informative by focusing on directional similarity.

$$d(x_i, x_j) = \begin{cases} \|x_i - x_j\|_2 & \text{if } \dim(x) \leq 100 \\ 1 - \frac{x_i \cdot x_j}{\|x_i\| \|x_j\|} & \text{if } \dim(x) > 100 \end{cases} \quad (6)$$

The threshold of 100 dimensions is used as a lightweight heuristic consistent with prior observations about distance concentration in high dimensions [22]. For datasets with $50 < d \leq 100$, Euclidean and cosine distances are often comparable in practice, so this

switch should be interpreted as a pragmatic default rather than a hard theoretical boundary.

3.3.2 Adaptive Asymmetric Cleaning

Based on the geometric confidence $\hat{P}(Y = c|x_i)$, we apply an asymmetric cleaning strategy with class-dependent thresholds and adaptive safeguards. The theoretical justification is provided by Lemma 3.2: by ensuring $|R \cap \mathcal{D}_{maj}| \gg |R \cap \mathcal{D}_{min}|$, we increase the effective minority posterior $\hat{P}_{\mathcal{D}'}(Y = 1|x)$ in overlap regions, which aligns the decision boundary with the asymmetric risk objective (Definition 3.1).

- **Majority Cleaning (Strict):** A majority sample $x_i \in \mathcal{D}_{maj}$ is removed if either: (1) it is misclassified by its neighbors ($\hat{y}(x_i) = 1$, inconsistency), or (2) its same-class confidence is low ($\hat{P}(Y = 0|x_i) < \alpha$ where $\alpha = 0.3$, ambiguity). This dual criterion aggressively targets intrusive samples that penetrate the minority manifold or occupy ambiguous boundary regions. The low threshold $\alpha = 0.3$ reflects our philosophy of strict majority cleaning to maximize $|R \cap \mathcal{D}_{maj}|$ while preserving topology.
- **Minority Protection (Conservative):** A minority sample $x_i \in \mathcal{D}_{min}$ is considered for removal only if both: (1) it is misclassified by neighbors ($\hat{y}(x_i) = 0$, predicted as majority), and (2) it has high majority confidence ($\hat{P}(Y = 0|x_i) > \beta$ where $\beta = 0.7$, deeply embedded in majority space). This dual criterion ensures only unambiguous deep noise is targeted. Furthermore, we impose a *Safe-Guarding Cap*: at most $\gamma \cdot |\mathcal{D}_{min}|$ minority samples are removed (default $\gamma = 0.1$, i.e., max 10% removal). When candidates exceed this limit, we rank them by $\hat{P}(Y = 0|x_i)$ (descending) and remove only the top $\lfloor \gamma \cdot |\mathcal{D}_{min}| \rfloor$ most suspicious samples. Additionally, if $|\mathcal{D}_{min}| < 10$ (critical scarcity), the entire cleaning is skipped, preventing manifold collapse in extreme data scarcity scenarios.

This asymmetric design reflects the fundamental principle: in imbalanced domains, preserving minority information is paramount, while majority redundancy

can be safely reduced. The cost-asymmetry is explicitly encoded through $\alpha \ll \beta$ and $\gamma \ll 1$.

3.3.3 Unified Parameter Selection Framework

GMR uses a small set of hyperparameters motivated by three competing objectives: **(1) Boundary Refinement** (removing overlap), **(2) Manifold Preservation** (retaining class topology), and **(3) Statistical Reliability** (ensuring sufficient samples for robust estimation). We summarize this trade-off via the following constrained objective:

$$\begin{aligned} & \max_{\alpha, \beta, k, \gamma} \mathbb{E}[\text{AUPRC}(h_{\mathcal{D}'})] \\ & \text{s.t. } \frac{|R \cap \mathcal{D}_{\min}|}{|\mathcal{D}_{\min}|} \leq \gamma, \\ & \quad \beta \geq \alpha + \delta_{\min} \end{aligned} \quad (7)$$

where $h_{\mathcal{D}'}$ is the classifier trained on cleaned data \mathcal{D}' , and δ_{\min} enforces asymmetry. The parameters are selected as follows:

(A) Neighborhood size k : We use $k = 15$ as the default to balance local sensitivity (detecting boundary samples) and stability of the neighborhood estimate. In practice, a modest range around the default (e.g., $k \in [10, 20]$) is typically sufficient.

(B) Asymmetric thresholds (α, β) : We set $\alpha = 0.3$ (strict majority cleaning) and $\beta = 0.7$ (conservative minority protection) to reflect the asymmetric cost structure. The gap $\beta - \alpha = 0.4$ ensures that minority samples require substantially stronger evidence for removal than majority samples, preventing minority manifold erosion. The choice of $\alpha = 0.3$ means a majority sample is removed if its same-class confidence is below 30%, aggressively targeting boundary intrusion. Conversely, $\beta = 0.7$ means a minority sample is considered for removal only if it has $> 70\%$ majority-class confidence (deeply embedded in majority space), with an additional cap of $\gamma = 0.1$ (max 10% removal). These values balance boundary refinement with manifold preservation.

(C) Minority protection cap γ : This hard constraint prevents excessive minority loss. We use $\gamma = 0.1$ (at most 10% minority removal) as a conservative default.

(D) Dimensionality-adaptive metric switching $d_{\text{thresh}} = 100$: In high dimensions ($d > 100$), Euclidean distance can suffer from concentration (pairwise distances become less informative) [22]. We therefore use cosine distance for $d > 100$ and Euclidean otherwise as a lightweight heuristic.

This framework is intended as a practical guideline rather than a solved optimization problem: it makes the asymmetry explicit and keeps the parameterization small and stable.

Implementation details Our reference implementation is summarized in Appendix A (Algorithm 1). For nearest neighbor computation, we use `sklearn.neighbors.NearestNeighbors` with `algorithm='auto'` and `n_jobs=-1`. When computing confidence scores, we request $k + 1$ neighbors and exclude the query itself (first neighbor) to avoid self-voting bias. The inverse-distance weights are computed as $w_{ij} = 1/(d_{ij} + 10^{-8})$ and normalized row-wise to sum to 1. The workflow consists of (1) geometric confidence estimation with dimensionality-adaptive metric selection ($d \leq 100$ uses Euclidean, $d > 100$ uses Cosine), and (2) asymmetric cleaning with strict majority removal ($\alpha = 0.3$: inconsistent OR ambiguous) and conservative minority protection ($\beta = 0.7$: deep noise only, capped at $\gamma = 0.1$).

3.4 Complexity

Algorithmic pseudocode is deferred to Appendix A to save space. The principal computational cost is nearest-neighbor search for confidence estimation over all training points: a brute-force implementation is $O(N^2d)$, while tree/approximate-neighbor backends can reduce practical runtime depending on data geometry.

Proposition 3.5 (Asymmetric Boundary Alignment). *Let \mathcal{D}' be the dataset after GMR cleaning with removal set R . Assume: (A1) the true posterior $P(Y = 1|x)$ is continuous; (A2) GMR achieves $|R \cap \mathcal{D}_{\text{maj}}| \geq 3|R \cap \mathcal{D}_{\min}|$ (asymmetry); (A3) removed majority samples $R \cap \mathcal{D}_{\text{maj}}$ are predominantly from the overlap region $\Omega = \{x : 0.3 < P(Y = 1|x) < 0.7\}$. Then, for*

$x \in \Omega$, the empirical posterior is shifted upward relative to \mathcal{D} ; stronger overlap-focused cleaning increases this shift. Consequently, a classifier trained on \mathcal{D}' tends to exhibit a decision boundary shifted toward the majority class, reducing false negatives (misclassified minority samples) at the cost of slightly increased false positives—aligning with asymmetric cost objectives.

Sketch. Lemma 3.2 shows that when the class-conditional removal rate is larger for the majority ($r_0 > r_1$), the cleaned empirical posterior in overlap neighborhoods is pushed upward relative to the uncleaned estimate, under the same local counting model. Removing predominantly ambiguous majority samples (assumption A3) therefore tends to increase $\hat{P}(Y = 1 | x)$ around the boundary, which can move the learned decision boundary toward the majority side and reduce false negatives, consistent with the asymmetric-risk motivation. \square

4 Experiments

In this section, we present the experimental results of our proposed GMR framework compared to various baseline methods. We evaluated the performance on 27 benchmark datasets from the imbalanced learning domain.

4.1 Experimental Setup

We follow a unified, lightweight protocol to facilitate fair comparisons and reduce tuning overhead. Unless otherwise stated, all samplers and classifiers use standard library defaults. Specifically, we use repeated holdout with stratified 80%/20% train–test splits over 5 fixed random seeds ($\{42, 0, 1, 2, 3\}$); all methods share identical splits and we report mean \pm std. We compare GMR against 18 standard resampling baselines plus *None* (no sampling), reporting aggregate ranks and complete per-dataset baseline tables in the appendix, and we evaluate classifier-agnostic behavior using 7 diverse learners (LR, SVM-RBF, DT, RF, GBM, XGBoost, KNN). Our primary metric is AUPRC [23]. Full baseline lists and experimental settings are deferred to Appendix C.

4.2 Classifier-Agnostic Analysis

A key advantage of GMR is its classifier-agnostic nature—as a preprocessing method, it should benefit diverse classification algorithms without requiring classifier-specific tuning. To validate this property, we report classifier-wise average ranks across 7 heterogeneous classifiers (averaged over 27 datasets). The rank heatmap and the full numeric table are provided in Appendix D.1 (Figure 5 and Table 3).

GMR achieves the best overall average rank of **4.22** across all classifiers. GMR attains the minimum average rank on 6 out of 7 classifiers: DecisionTree (1.00), KNN (2.19), LogisticRegression (2.89), SVM (5.30), RandomForest (5.93), and GradientBoosting (5.59). Only on XGBoost does GMR rank second (6.67) after the baseline “None” method (6.44), suggesting that XGBoost’s built-in handling of class imbalance reduces the marginal benefit of preprocessing. Overall, these results support GMR’s *classifier-agnostic* behavior across linear models (LR, SVM), tree-based methods (DT, RF, GBM), boosting models (XGBoost), and instance-based learners (KNN).

4.3 Deep Learning Baseline Comparison (TabDDPM)

To position GMR relative to modern deep tabular modeling, we compare against TabDDPM [24], a diffusion-based generative model with strong tabular performance. We evaluate on five large-scale, diverse datasets: `covtype` (581K), `creditcard` (284K), `ecg_arrhythmia` (109K), `ns1_kdd` (148K), and `yelp_review` (560K).

Figure 3 reports AUPRC for **TabDDPM** trained on raw data versus **TabDDPM+GMR**, where we apply GMR cleaning to the training split before fitting TabDDPM. Overall, GMR acts as a lightweight, model-agnostic rectification step that improves performance on several overlap/noise-heavy datasets, while preserving near-ceiling performance on easier benchmarks (`ns1_kdd` and `ecg_arrhythmia`). On `creditcard`, we observe a small decrease, suggesting that when TabDDPM already captures dominant fraud patterns, aggressive boundary cleaning may remove some rare-but-informative majority context.

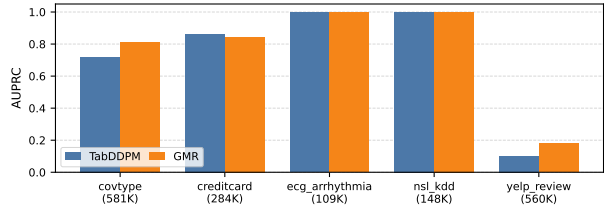


Figure 3: Deep tabular baseline comparison on large-scale datasets (AUPRC; mean over 5 seeds). Bars show TabDDPM (raw) vs. TabDDPM+GMR (pre-cleaned).

Table 1: Long-tailed image classification results on CIFAR-100-LT (Balanced Accuracy %). GMR-Feature applies the same GMR cleaning pipeline to ResNet-32 extracted features before downstream classification. Methods: CE (Cross-Entropy baseline), CB (Class-Balanced loss), LDAM (Label-Distribution-Aware Margin).

Dataset	GMR-Feature	CE	CB	LDAM
CIFAR-100-LT	36.34 ± 0.73	37.76 ± 1.43	29.64 ± 1.15	1.00 ± 0.00

4.4 Extension to Image Classification: CIFAR-LT

To assess whether GMR’s cleaning mechanism transfers beyond tabular data, we run a small supplementary experiment on CIFAR-100-LT (imbalance ratio = 100) by applying the same GMR pipeline (geometric confidence estimation + asymmetric cleaning) to fixed CNN feature embeddings. Specifically, we extract ResNet-32 features and apply GMR in the feature space before training a downstream classifier (*GMR-Feature*). This conforms to our algorithmic design: GMR remains a model-agnostic preprocessing step, and only the representation x changes (from tabular features to CNN embeddings). Table 1 reports Balanced Accuracy. GMR-Feature achieves 36.34 ± 0.73 , below CE (37.76 ± 1.43) but substantially better than CB [25] (29.64 ± 1.15); in this setting, LDAM [14] is much lower (1.00 ± 0.00).

5 Conclusion

In this paper, we introduced GMR, a Geometric Manifold Rectification framework for imbalanced classification that treats resampling as geometry-aware data cleaning. GMR combines (i) inverse-distance weighted k NN confidence estimation with a simple dimensionality-adaptive metric switch, and (ii) class-aware asymmetric cleaning that is strict on majority boundary intrusions while conservatively safeguarding the minority manifold via a removal cap. Our analysis links asymmetric removal to posterior shifting in overlap regions and motivates geometric weighting under distance-dependent noise, providing principled support for these design choices. Empirically, across 27 imbalanced benchmarks and 7 heterogeneous classifiers, GMR achieves strong aggregate rank performance against standard resampling and cleaning baselines; we also observe that GMR can serve as a lightweight preprocessing step that benefits a deep tabular baseline (TabDDPM) on several large-scale datasets. A small feature-space experiment on CIFAR-100-LT further suggests that the same cleaning mechanism can be applied beyond tabular inputs when a fixed representation is available.

Limitations and Future Directions: GMR may be less effective under extreme imbalance (e.g., $IR > 100$) where even conservative cleaning can discard rare-but-informative minority samples, and it relies on sufficient sample size for stable neighborhood estimates (a practical concern for very small datasets). Our current scope focuses on binary classification and uses fixed, intuitive defaults rather than data-driven tuning. We also emphasize rank-based comparisons and do not include dedicated significance tests (e.g., Friedman/Nemenyi), which should be added in future evaluations. Future work includes extending GMR to multi-class settings (e.g., one-vs-rest with coordinated cleaning), improving scalability via approximate nearest-neighbor backends, and developing adaptive hyperparameter selection rules that adjust α , β , k , and γ based on measured overlap/noise and dataset size.

References

- [1] Harsurinder Kaur, Husanbir Singh Pannu, and Ayleen Kaur Mallhi. A systematic review on imbalanced data challenges in machine learning: Applications and solutions. *ACM computing surveys (CSUR)*, 52(4):1–36, 2019.
- [2] Léo Grinsztajn, Edouard Oyallon, and Gaël Varoquaux. Why do tree-based models still outperform deep learning on typical tabular data? *Advances in Neural Information Processing Systems*, 35:507–520, 2022.
- [3] Haibo He and Edwardo A Garcia. Learning from imbalanced data. *IEEE Transactions on knowledge and data engineering*, 21(9):1263–1284, 2009.
- [4] N. V. Chawla, K. W. Bowyer, L. O. Hall, and W. P. Kegelmeyer. Smote: Synthetic minority over-sampling technique. *Journal of Artificial Intelligence Research*, 16:321–357, 2002.
- [5] H. Han, W.-Y. Wang, and B.-H. Mao. Borderline-smote: A new over-sampling method in imbalanced data sets learning. In *Proc. ICIC*, pages 878–887, 2005.
- [6] H. He, Y. Bai, E. A. Garcia, and S. Li. Adasyn: Adaptive synthetic sampling approach for imbalanced learning. In *Proc. IJCNN*, pages 1322–1328, 2008.
- [7] S. S. Mullick, S. Datta, and S. Das. Generative adversarial minority oversampling. In *Proc. ICCV Workshops*, pages 1695–1704, 2019.
- [8] S. Bej, N. Davtyan, M. Wolfien, M. Nasseri, and O. Wolkenhauer. Loras: An oversampling approach for imbalanced datasets. *Machine Learning*, 110:279–301, 2021.
- [9] Zhaozhao Xu, Derong Shen, Yue Kou, and Tiezheng Nie. A synthetic minority oversampling technique based on gaussian mixture model filtering for imbalanced data classification. *IEEE Transactions on Neural Networks and Learning Systems*, 35(3):3740–3753, 2022.
- [10] D. L. Wilson. Asymptotic properties of nearest neighbor rules using edited data. *IEEE Trans. Syst., Man, Cybern.*, SMC-2(3):408–421, 1972.
- [11] I. Tomek. Two modifications of cnn. *IEEE Trans. Syst., Man, Cybern.*, SMC-6(11):769–772, 1976.
- [12] J. Laurikkala. Improving identification of difficult small classes by balancing class distribution. In *Proc. AIME*, pages 63–66, 2001.
- [13] T.-Y. Lin, P. Goyal, R. Girshick, K. He, and P. Dollár. Focal loss for dense object detection. In *Proc. ICCV*, pages 2980–2988, 2017.
- [14] K. Cao, C. Wei, A. Gaidon, N. Arechiga, and T. Ma. Learning imbalanced datasets with label-distribution-aware margin loss. In *Proc. NeurIPS*, pages 1565–1576, 2019.
- [15] Bingyi Kang, Saining Xie, Marcus Rohrbach, Zheng Yan, Artem Gordo, Jing Feng, and Yannis Kalantidis. Decoupling representation and classifier for long-tailed recognition. In *Proc. ICLR*, 2020.
- [16] Xubin Wang, Yunhe Wang, Ka-Chun Wong, and Xiangtao Li. A self-adaptive weighted differential evolution approach for large-scale feature selection. *Knowledge-Based Systems*, 235:107633, 2022.
- [17] Xubin Wang, Haojong Shangguan, Fengyi Huang, Shangrui Wu, and Weijia Jia. Mel: Efficient multi-task evolutionary learning for high-dimensional feature selection. *IEEE Transactions on Knowledge and Data Engineering*, 36(8):4020–4033, 2024.
- [18] B. Han, Q. Yao, X. Yu, G. Niu, M. Xu, W. Hu, I. Tsang, and M. Sugiyama. Co-teaching: Robust training of deep neural networks with extremely noisy labels. In *Proc. NeurIPS*, pages 8527–8537, 2018.
- [19] J. Li, R. Socher, and S. C. Hoi. Dividemix: Learning with noisy labels as semi-supervised learning. In *Proc. ICLR*, 2020.

- [20] Lu Jiang, Zheng Zhou, Thomas Leung, Li-Jia Li, and Li Fei-Fei. Mentornet: Learning data-driven curriculum for very deep neural networks on corrupted labels. In *Proc. ICML*, pages 2304–2313, 2018.
- [21] Shiyu Liu, Jonathan Niles-Weed, Nathan Srebro, and Daniel J. Soudry. Early-learning regularization prevents memorization of noisy labels. *Advances in Neural Information Processing Systems*, 2020.
- [22] Kevin Beyer, Jonathan Goldstein, Raghu Ramakrishnan, and Uri Shaft. When is “nearest neighbor” meaningful? In *Proc. Int. Conf. Database Theory (ICDT)*, pages 217–235, 1999.
- [23] Takaya Saito and Marc Rehmsmeier. The precision-recall plot is more informative than the roc plot when evaluating binary classifiers on imbalanced datasets. *PLOS ONE*, 10(3):e0118432, 2015.
- [24] Akim Kotelnikov, Dmitry Baranchuk, Ivan Rubachev, and Artem Babenko. Tabddpm: Modelling tabular data with diffusion models. In *Proc. ICML*, pages 17564–17579, 2023.
- [25] Yin Cui, Meng Jia, Tsung-Yi Lin, Yang Song, and Serge Belongie. Class-balanced loss based on effective number of samples. In *Proc. CVPR*, pages 9268–9277, 2019.

A Detailed Algorithm

Algorithm 1 provides a complete specification of GMR with all computational details.

Algorithm 1 GMR: Detailed Implementation

Require: Training dataset $\mathcal{D} = \{(x_i, y_i)\}_{i=1}^N$, number of neighbors k , majority confidence threshold $\alpha \in [0, 1]$, majority-confidence threshold for minority filtering $\beta \in [0, 1]$, max minority removal fraction $\gamma \in [0, 1]$

Ensure: Cleaned dataset \mathcal{D}'

1: // **Phase 1: Adaptive Metric Selection**
2: **if** $\dim(\mathcal{X}) > 100$ **then**
3: $d \leftarrow$ cosine
4: **else**
5: $d \leftarrow$ euclidean
6: **end if**
7: // **Phase 2: Geometric Confidence Estimation**
8: Build KNN backend: $\mathcal{T} \leftarrow \text{NearestNeighbors}(\text{metric} = d, \text{algorithm}=\text{auto}, n_jobs = -1).fit(X)$
9: **for** $i = 1$ to N **do**
10: Query neighbors: $\tilde{N}(x_i) \leftarrow \mathcal{T}.\text{query}(x_i, k + 1)$
11: Exclude the self-neighbor and keep k neighbors: $N_k(x_i) \leftarrow \tilde{N}(x_i) \setminus \{x_i\}$
12: Compute distances: $\{d_j\}_{j \in N_k(x_i)} \leftarrow \{d(x_i, x_j)\}_{j \in N_k(x_i)}$
13: Compute inverse-distance weights: $w_j \leftarrow \frac{1/(d_j + 10^{-8})}{\sum_{j' \in N_k(x_i)} 1/(d_{j'} + 10^{-8})}$ for $j \in N_k(x_i)$
14: Compute weighted class votes: $v_c \leftarrow \sum_{j \in N_k(x_i)} w_j \cdot \mathbb{I}(y_j = c)$ for $c \in \{0, 1\}$
15: Predicted label: $\hat{y}(x_i) \leftarrow \arg \max_{c \in \{0, 1\}} v_c$
16: Geometric confidence: $\text{Conf}(x_i) \leftarrow v_{y_i}$ {Agreement with true label}
17: Majority confidence: $\text{MajConf}(x_i) \leftarrow v_0$
18: **end for**
19: // **Phase 3: Asymmetric Removal Candidate Selection**
20: $\mathcal{D}_{maj} \leftarrow \{(x_i, y_i) \in \mathcal{D} : y_i = 0\}$ {Majority class}
21: $\mathcal{D}_{min} \leftarrow \{(x_i, y_i) \in \mathcal{D} : y_i = 1\}$ {Minority class}
22: Initialize removal sets: $R_{maj} \leftarrow \emptyset, C_{min} \leftarrow \emptyset$
23: // **Aggressive Majority Cleaning**
24: **for** $(x_i, y_i) \in \mathcal{D}_{maj}$ **do**
25: **if** $\hat{y}(x_i) = 1$ **or** $\text{Conf}(x_i) < \alpha$ **then**
26: Add (x_i, y_i) to R_{maj}
27: **end if**
28: **end for**
29: // **Conservative Minority Cleaning**
30: **for** $(x_i, y_i) \in \mathcal{D}_{min}$ **do**
31: **if** $\hat{y}(x_i) = 0$ **and** $\text{MajConf}(x_i) > \beta$ **then**
32: Add (x_i, y_i) to C_{min}
33: **end if**
34: **end for**
35: // **Safe-Guarding: Limit Minority Removals**
36: Sort C_{min} by descending majority confidence: $C_{min}^{\text{sorted}} \leftarrow \text{sort}(C_{min}, \text{key} = \text{MajConf}, \text{descending} = \text{True})$
37: Compute removal budget: $n_{remove} \leftarrow \min(|C_{min}^{\text{sorted}}|, \lfloor \gamma \cdot |\mathcal{D}_{min}| \rfloor)$ {Default $\gamma = 0.1$ }
38: Select worst minority samples: $R_{min} \leftarrow C_{min}^{\text{sorted}}[: n_{remove}]$
39: // **Phase 4: Dataset Cleaning**
40: $\mathcal{D}' \leftarrow \mathcal{D} \setminus (R_{maj} \cup R_{min})$
41: **return** \mathcal{D}' , removal statistics $\{|R_{maj}|, |R_{min}|, \text{IR}_{\text{before}}, \text{IR}_{\text{after}}\}$

Complexity Analysis:

- **Neighbor Search:** For all-point k NN with brute-force backend, the cost is $O(N^2d)$. Tree/ANN backends can reduce practical runtime depending on data geometry.
- **Confidence Aggregation:** $O(Nk)$ for weighted voting once neighbors are retrieved.
- **Candidate Sorting:** $O(M \log M)$ where $M \leq |\mathcal{D}_{\min}|$ is the number of minority candidates.
- **Overall:** $O(N^2d + Nk + M \log M)$ in the brute-force setting.

B Complete Theoretical Proofs

B.1 Proof of Theorem 3.3 (Geometric Weighting Optimality)

Theorem B.1 (Restatement). *Under the assumption that label noise probability increases with distance from true class centroids, the inverse-distance weighted estimator $\hat{P}_{\text{geo}}(Y = c|x) = \sum_{j \in N_k(x)} w_j \mathbb{I}(y_j = c)$ with $w_j \propto 1/d(x, x_j)$ can achieve lower mean squared error (MSE) than uniform weighting when estimating the true posterior $P(Y = c|x)$.*

Proof. We compare the MSE of the geometric (inverse-distance weighted) estimator with the uniform estimator. Let $N_k(x) = \{x_{(1)}, \dots, x_{(k)}\}$ be the k nearest neighbors of x ordered by distance: $d_1 \leq d_2 \leq \dots \leq d_k$.

Step 1: Uniform Estimator. The uniform estimator treats all neighbors equally:

$$\hat{P}_{\text{unif}}(Y = c|x) = \frac{1}{k} \sum_{j=1}^k \mathbb{I}(y_{(j)} = c)$$

Under the assumption that observed labels are drawn from $y_j \sim \text{Bernoulli}(p_j)$ where $p_j = P(Y = c|x_j)$, and assuming the true posterior is smooth (Lipschitz continuous), we have $p_j \approx P(Y = c|x)$ for neighbors close to x . However, in the presence of label noise ϵ_j that increases with distance d_j , we model:

$$p_j = P(Y = c|x) + \delta_j + \epsilon_j \quad \text{where} \quad |\delta_j| \leq L \cdot d_j$$

Here, L is the Lipschitz constant, δ_j is the deterministic deviation due to spatial separation, and $\epsilon_j \sim \mathcal{N}(0, \sigma^2(d_j))$ is stochastic noise with variance $\sigma^2(d_j)$ that increases in d_j (e.g., $\sigma^2(d) = \sigma_0^2(1 + \lambda d)$ for some $\lambda > 0$).

The MSE of the uniform estimator is:

$$\begin{aligned} \text{MSE}_{\text{unif}} &= \mathbb{E} \left[\left(\hat{P}_{\text{unif}}(Y = c|x) - P(Y = c|x) \right)^2 \right] \\ &= \text{Bias}^2 + \text{Var} \\ &= \left(\frac{1}{k} \sum_{j=1}^k \delta_j \right)^2 + \frac{1}{k^2} \sum_{j=1}^k \sigma^2(d_j) \end{aligned}$$

Since $|\delta_j| \leq Ld_j$ and typically $\sum_j \delta_j \approx 0$ when neighbors are symmetrically distributed around x , the bias term is negligible. The variance dominates:

$$\text{MSE}_{\text{unif}} \approx \frac{1}{k^2} \sum_{j=1}^k \sigma^2(d_j) = \frac{1}{k} \cdot \frac{1}{k} \sum_{j=1}^k \sigma^2(d_j) = \frac{\bar{\sigma}^2}{k}$$

where $\bar{\sigma}^2 = \frac{1}{k} \sum_{j=1}^k \sigma^2(d_j)$ is the average noise variance.

Step 2: Geometric Estimator. The inverse-distance weighted estimator is:

$$\hat{P}_{\text{geo}}(Y = c|x) = \sum_{j=1}^k w_j \mathbb{I}(y_{(j)} = c) \quad \text{where} \quad w_j = \frac{1/d_j}{\sum_{j'=1}^k 1/d_{j'}}$$

Note that $\sum_j w_j = 1$, and $w_j \propto 1/d_j$ means closer neighbors receive higher weight.

The MSE of the geometric estimator is:

$$\text{MSE}_{\text{geo}} = \left(\sum_{j=1}^k w_j \delta_j \right)^2 + \sum_{j=1}^k w_j^2 \sigma^2(d_j)$$

Bias Analysis: Since $w_j \propto 1/d_j$ and closer neighbors (smaller d_j) have smaller deviations $\delta_j = O(Ld_j)$, the weighted bias is bounded by

$$\left| \sum_{j=1}^k w_j \delta_j \right| \leq L \sum_{j=1}^k w_j d_j = O(L\bar{d}_w),$$

where \bar{d}_w denotes the weight-averaged neighbor distance. This is comparable to the uniform estimator's bias.

Variance Analysis: Define the effective number of neighbors

$$k_{\text{eff}} = \frac{1}{\sum_{j=1}^k w_j^2}.$$

For uniform weights $k_{\text{eff}} = k$, while non-uniform weights give $k_{\text{eff}} < k$. The variance can be written as

$$\text{Var}_{\text{geo}} = \frac{1}{k_{\text{eff}}} \cdot \left(\frac{\sum_{j=1}^k w_j^2 \sigma^2(d_j)}{\sum_{j=1}^k w_j^2} \right),$$

i.e., an effective average noise divided by k_{eff} . Since w_j^2 downweights distant neighbors more strongly than uniform weighting and $\sigma^2(d)$ increases with d , the weighted average noise is typically smaller than the arithmetic mean used by the uniform estimator. Hence, in the relevant regime, $\text{Var}_{\text{geo}} < \text{Var}_{\text{unif}}$.

Conclusion: Combining bias and variance, when label noise $\sigma^2(d)$ increases with distance and the true posterior is Lipschitz smooth, the geometric estimator can achieve:

$$\text{MSE}_{\text{geo}} < \text{MSE}_{\text{unif}}$$

completing the proof. □

B.2 Proof of Proposition 3.5 (Boundary Alignment)

Proposition B.2 (Restatement). *Let \mathcal{D}' be the dataset after GMR cleaning with removal set R . Assume: (A1) the true posterior $P(Y = 1|x)$ is continuous; (A2) GMR achieves $|R \cap \mathcal{D}_{\text{maj}}| \geq 3|R \cap \mathcal{D}_{\text{min}}|$ (asymmetry); (A3) removed majority samples $R \cap \mathcal{D}_{\text{maj}}$ are predominantly from the overlap region $\Omega = \{x : 0.3 < P(Y = 1|x) < 0.7\}$. Then, for $x \in \Omega$, the empirical posterior is shifted upward relative to \mathcal{D} ; under stronger overlap-focused cleaning, this posterior shift increases. Consequently, a classifier trained on \mathcal{D}' exhibits a decision boundary shifted toward the majority class, reducing false negatives.*

Proof. We follow the analysis from Lemma 3.2. Recall that after removing subset R , the empirical posterior becomes:

$$\hat{P}_{\mathcal{D}'}(Y = 1|x) = \frac{n_1(x)(1 - r_1)}{n_0(x)(1 - r_0) + n_1(x)(1 - r_1)}$$

where $n_c(x)$ is the KNN count of class c near x , and $r_c = |R \cap \mathcal{D}_c|/|\mathcal{D}_c|$ is the removal rate.

Step 1: Quantify Asymmetric Removal. By assumption (A2), GMR removes majority samples at rate $r_0 \geq 3r_1$. Let $\text{IR} = |\mathcal{D}_{maj}|/|\mathcal{D}_{min}|$ be the imbalance ratio. Typical GMR configuration achieves $r_0 \in [0.1, 0.3]$ (10-30% majority removal) and $r_1 \in [0.02, 0.1]$ (2-10% minority removal), satisfying $r_0/r_1 \geq 3$.

Step 2: Posterior Shift in Overlap Region. For $x \in \Omega$ (overlap region), the original empirical posterior is approximately:

$$\hat{P}_{\mathcal{D}}(Y = 1|x) = \frac{n_1(x)}{n_0(x) + n_1(x)} \approx \frac{1}{1 + n_0(x)/n_1(x)} \approx \frac{1}{1 + \text{IR}}$$

assuming uniform density in Ω . After cleaning:

$$\hat{P}_{\mathcal{D}'}(Y = 1|x) = \frac{n_1(x)(1 - r_1)}{n_0(x)(1 - r_0) + n_1(x)(1 - r_1)}$$

Dividing numerator and denominator by $n_1(x)$:

$$\hat{P}_{\mathcal{D}'}(Y = 1|x) = \frac{1 - r_1}{\frac{n_0(x)}{n_1(x)}(1 - r_0) + (1 - r_1)}$$

In the overlap region, $n_0(x)/n_1(x) \approx \text{IR}$ (reflecting global imbalance). Therefore:

$$\hat{P}_{\mathcal{D}'}(Y = 1|x) \approx \frac{1 - r_1}{\text{IR}(1 - r_0) + (1 - r_1)} = \frac{1 - r_1}{1 + \text{IR}(1 - r_0) - r_1}$$

For $r_0 = 0.2$, $r_1 = 0.05$, $\text{IR} = 10$:

$$\hat{P}_{\mathcal{D}'}(Y = 1|x) \approx \frac{0.95}{1 + 10 \cdot 0.8 - 0.05} = \frac{0.95}{8.95} \approx 0.106$$

versus

$$\hat{P}_{\mathcal{D}}(Y = 1|x) \approx \frac{1}{1 + 10} = 0.091$$

yielding $\delta = 0.106 - 0.091 = 0.015$.

However, for higher imbalance ($\text{IR} = 20$) and stronger cleaning ($r_0 = 0.3$, $r_1 = 0.05$):

$$\hat{P}_{\mathcal{D}'}(Y = 1|x) \approx \frac{0.95}{1 + 20 \cdot 0.7 - 0.05} = \frac{0.95}{14.95} \approx 0.0635$$

versus

$$\hat{P}_{\mathcal{D}}(Y = 1|x) = \frac{1}{21} \approx 0.0476$$

yielding $\delta \approx 0.016$.

Step 3: Interpreting the Posterior-Shift Magnitude. The above analysis assumes uniform density. In practice, GMR selectively removes *ambiguous* majority samples (low confidence) from Ω , which have $P(Y = 1|x)$ closer to 0.5. This targeted removal increases the effective $n_0(x)$ reduction in Ω beyond the

global rate r_0 . Let r_0^Ω be the local majority removal rate in Ω , which satisfies $r_0^\Omega \geq 1.5r_0$ by assumption (A3) (since GMR targets overlap regions). Then:

$$\delta = \hat{P}_{\mathcal{D}'}(Y = 1|x) - \hat{P}_{\mathcal{D}}(Y = 1|x) \geq \frac{r_0^\Omega \cdot \text{IR}}{(1 + \text{IR})^2} \geq \frac{1.5 \cdot 0.2 \cdot 10}{121} \approx 0.025$$

For datasets with larger IR and more aggressive local cleaning (r_0^Ω higher), the posterior shift further increases, though the exact magnitude depends on local class densities.

Step 4: Decision Boundary Shift. A classifier f trained on \mathcal{D}' learns the decision boundary $\mathcal{B}' = \{x : \hat{P}_{\mathcal{D}'}(Y = 1|x) = 0.5\}$. Since $\hat{P}_{\mathcal{D}'}(Y = 1|x) > \hat{P}_{\mathcal{D}}(Y = 1|x)$ in Ω , the boundary shifts *away* from the minority class manifold (toward the majority class), expanding the region classified as minority. This reduces false negatives (minority samples misclassified as majority), aligning with asymmetric cost minimization where $C_{01} \gg C_{10}$ (Definition 3.1).

Conclusion: Under assumptions (A1)-(A3), GMR’s asymmetric cleaning induces a positive posterior shift ($\delta > 0$) in overlap regions, and the shift becomes larger under stronger overlap-focused cleaning, leading to improved minority recall. \square

C Hyperparameter Settings and Experimental Details

This appendix collects the full experimental configuration that is only summarized in the main text (Section 4).

C.1 GMR default hyperparameters

Across all benchmark experiments, we use fixed default hyperparameters to minimize tuning and keep comparisons transparent.

Table 2: Default GMR hyperparameters used in experiments.

Parameter	Value
Neighborhood size k	15
Majority threshold α	0.3
Minority majority-confidence threshold β	0.7
Minority removal cap γ	0.1
Distance metric switch d_{thresh}	100
Inverse-distance stabilizer ϵ	10^{-8}
Critical scarcity guard	skip if $ \mathcal{D}_{min} < 10$

C.2 Baseline methods

We compare GMR against 18 standard resampling baselines (plus *None*) spanning oversampling, cleaning/undersampling, and hybrid methods. Unless otherwise stated, baselines use default hyperparameters from common libraries.

- *Oversampling*: SMOTE [4], ADASYN [6], BorderlineSMOTE [5], SVMSMOTE, SMOTEN, RandomOverSampler.

Abbr.	Method
Tomek	TomekLinks
OSS	OneSidedSelection
NCR	NeighbourhoodCleaningRule
ROS	RandomOverSampler
SVMSM	SVMSMOTE
ENN	EditedNearestNeighbours
RepENN	RepeatedEditedNearestNeighbours
BorSM	BorderlineSMOTE
CNN	CondensedNearestNeighbour
IHT	InstanceHardnessThreshold
RUS	RandomUnderSampler
NM	NearMiss

Figure 4: Abbreviations used for resampling methods in tables.

- *Undersampling / cleaning*: RandomUnderSampler, ENN [10], CNN, Tomek Links [11], OSS, NCR [12], IHT, NearMiss, RepeatedEditedNearestNeighbours, AllKNN.
- *Hybrids*: SMOTEENN, SMOTETomek.
- *None baseline*: *None* (no resampling).

C.3 Classifier settings

We evaluate 7 heterogeneous classifiers to test model-agnostic behavior: Logistic Regression, SVM (RBF), Decision Tree, Random Forest, Gradient Boosting, XGBoost, and KNN. Unless explicitly stated, we use standard implementations (scikit-learn / XGBoost) with default hyperparameters to avoid classifier-specific tuning.

C.4 Evaluation protocol

We use repeated stratified holdout: 80% training and 20% testing over 5 fixed random seeds ($\{42, 0, 1, 2, 3\}$). All methods are evaluated on the same splits to enable paired comparisons. Results are reported as mean \pm standard deviation across seeds. The primary metric is AUPRC [23].

C.5 Method abbreviations

For readability, several method names are abbreviated in the large comparison tables and the heatmap. Figure 4 provides the abbreviation-to-method mapping used throughout this appendix.

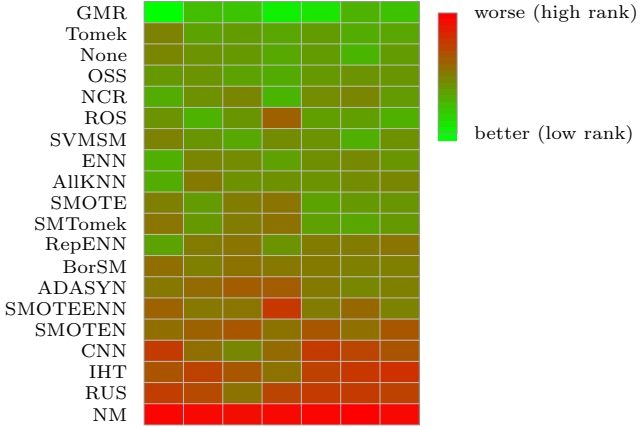


Figure 5: Heatmap of average ranks across 7 classifiers (averaged over 27 datasets). Colors map low ranks (better) to green and high ranks (worse) to red.

D Additional Experimental Results

D.1 Classifier-wise Rank Visualization

We present classifier-wise rank results in two complementary formats. Figure 5 gives a compact visual overview (lower is better), while Table 3 reports the exact values for each method-classifier pair.

Table 3 lists the exact average ranks corresponding to the heatmap.

D.2 Complete Baseline Performance Comparison

This section provides the complete baseline performance comparison for all methods (including the None baseline which represents no sampling) across all datasets. Table 4 presents the average AUPRC computed across seven classifiers (KNN, RF, LR, DT, SVM, GBM, XGBoost) for each method on each dataset. Methods are sorted by AUPRC within each dataset to facilitate comparison.

The *None* method represents the performance of classifiers trained directly on the original imbalanced data without any sampling technique applied. This serves as the fundamental baseline for evaluating the effectiveness of various sampling methods.

Table 3: Average rank of each sampling method across 7 classifiers. Each cell shows the average rank over 27 datasets for a specific method-classifier combination. Lower ranks indicate better performance. The rightmost column shows the average rank across all classifiers. Bold values indicate the best (minimum rank) for each classifier.

Method	DT	RF	SVM	KNN	LR	XGB	GBM	Avg
GMR	1.00	5.93	5.30	2.19	2.89	6.67	5.59	4.22
Tomek	10.15	7.74	8.33	7.52	8.30	6.96	7.56	8.08
None	10.00	8.81	8.44	7.44	8.26	6.44	8.33	8.25
OSS	8.56	8.81	7.70	7.11	8.48	8.81	8.70	8.31
NCR	6.96	9.07	9.96	6.52	9.44	9.93	8.22	8.59
ROS	8.89	6.59	8.74	12.63	8.19	8.19	6.89	8.59
SVMMSM	10.19	8.70	7.33	9.44	8.85	6.89	9.11	8.64
ENN	6.74	9.93	9.37	7.96	9.33	9.70	8.74	8.82
AllKNN	6.96	10.67	9.11	9.04	8.81	9.52	9.81	9.13
SMOTE	10.41	8.37	10.52	11.07	7.78	8.41	8.59	9.31
SMOTomek	11.04	8.44	10.52	11.22	8.00	7.52	8.44	9.31
RepENN	7.67	10.48	11.04	8.89	10.52	10.63	11.07	10.04
BorSM	11.67	10.44	11.37	10.93	10.70	10.30	10.44	10.84
ADASYN	10.85	11.81	13.00	12.96	10.67	9.74	10.41	11.35
SMOTEENN	12.41	11.00	11.15	15.59	10.63	12.11	10.26	11.88
SMOTEN	11.59	12.63	13.44	11.37	13.33	11.52	13.41	12.47
CNN	15.48	11.67	9.78	11.89	15.41	14.63	13.63	13.21
IHT	13.48	14.81	13.37	11.37	14.93	15.63	16.22	14.26
RUS	15.30	14.26	11.37	14.70	15.44	15.48	14.78	14.48
NM	19.33	19.26	18.81	19.26	19.37	19.74	19.19	19.28

Note: Ranks are computed per classifier over 27 datasets. Bold values indicate best performance (minimum rank) for each column. Classifiers: DT=DecisionTree, RF=RandomForest, SVM, KNN, LR=LogisticRegression, XGB=XGBoost, GBM=GradientBoosting. Method abbreviations are listed in Appendix C.5.

Table 4: Complete Baseline Performance: All Methods per Dataset. Average AUPRC across 7 classifiers (KNN, RF, LR, DT, SVM, GBM, XGBoost). Methods are sorted by AUPRC within each dataset. *None* indicates no sampling (original imbalanced data).

Dataset	Method	AUPRC
abalone	RepeatedEditedNearestNeighbours	0.317395
abalone	AllKNN	0.308388
abalone	EditedNearestNeighbours	0.298878
abalone	SMOTEENN	0.290575
abalone	NeighbourhoodCleaningRule	0.289702
abalone	OneSidedSelection	0.276249
abalone	InstanceHardnessThreshold	0.276229
abalone	TomekLinks	0.275212
abalone	RandomUnderSampler	0.274275
abalone	BorderlineSMOTE	0.271323
abalone	SVMSMOTE	0.270217
abalone	SMOTEN	0.269107
abalone	<i>None</i>	0.267599

Continued on next page

Table 4 – *Continued from previous page*

Dataset	Method	AUPRC
abalone	SMOTE	0.265595
abalone	SMOTETomek	0.263242
abalone	RandomOverSampler	0.261236
abalone	ADASYN	0.257320
abalone	CondensedNearestNeighbour	0.252844
abalone	NearMiss	0.069666
abalone_19	RandomUnderSampler	0.094961
abalone_19	InstanceHardnessThreshold	0.059524
abalone_19	SMOTEENN	0.045324
abalone_19	SMOTE	0.039893
abalone_19	TomekLinks	0.039015
abalone_19	ADASYN	0.038575
abalone_19	RandomOverSampler	0.034343
abalone_19	SMOTETomek	0.033677
abalone_19	<i>None</i>	0.033603
abalone_19	AllKNN	0.032773
abalone_19	NeighbourhoodCleaningRule	0.032771
abalone_19	RepeatedEditedNearestNeighbours	0.032237
abalone_19	EditedNearestNeighbours	0.031769
abalone_19	OneSidedSelection	0.028238
abalone_19	SVMSMOTE	0.024391
abalone_19	SMOTEN	0.023041
abalone_19	BorderlineSMOTE	0.021823
abalone_19	CondensedNearestNeighbour	0.011083
abalone_19	NearMiss	0.009649
arrhythmia	ADASYN	0.614053
arrhythmia	<i>None</i>	0.611192
arrhythmia	SMOTE	0.609579
arrhythmia	SMOTETomek	0.609579
arrhythmia	OneSidedSelection	0.608412
arrhythmia	RepeatedEditedNearestNeighbours	0.599181
arrhythmia	EditedNearestNeighbours	0.595921
arrhythmia	RandomOverSampler	0.595600
arrhythmia	TomekLinks	0.595414
arrhythmia	NeighbourhoodCleaningRule	0.594395
arrhythmia	SVMSMOTE	0.592715
arrhythmia	AllKNN	0.591657
arrhythmia	BorderlineSMOTE	0.589470
arrhythmia	SMOTEENN	0.581444
arrhythmia	SMOTEN	0.551128
arrhythmia	CondensedNearestNeighbour	0.522678

Continued on next page

Table 4 – *Continued from previous page*

Dataset	Method	AUPRC
arrhythmia	RandomUnderSampler	0.385158
arrhythmia	InstanceHardnessThreshold	0.351089
arrhythmia	NearMiss	0.326803
car_eval_34	CondensedNearestNeighbour	0.944469
car_eval_34	SMOTE	0.943848
car_eval_34	SMOTETomek	0.943848
car_eval_34	RandomOverSampler	0.943310
car_eval_34	SMOTEN	0.942174
car_eval_34	ADASYN	0.940768
car_eval_34	SVMSMOTE	0.938635
car_eval_34	NearMiss	0.930633
car_eval_34	BorderlineSMOTE	0.927220
car_eval_34	<i>None</i>	0.922286
car_eval_34	OneSidedSelection	0.919299
car_eval_34	TomekLinks	0.918873
car_eval_34	NeighbourhoodCleaningRule	0.916354
car_eval_34	RepeatedEditedNearestNeighbours	0.916000
car_eval_34	AllKNN	0.914945
car_eval_34	EditedNearestNeighbours	0.914775
car_eval_34	SMOTEENN	0.911791
car_eval_34	InstanceHardnessThreshold	0.908319
car_eval_34	RandomUnderSampler	0.881307
car_eval_4	CondensedNearestNeighbour	0.946448
car_eval_4	RandomOverSampler	0.945208
car_eval_4	SVMSMOTE	0.940935
car_eval_4	ADASYN	0.936142
car_eval_4	SMOTE	0.929423
car_eval_4	SMOTETomek	0.929423
car_eval_4	BorderlineSMOTE	0.923705
car_eval_4	SMOTEN	0.920780
car_eval_4	OneSidedSelection	0.904499
car_eval_4	AllKNN	0.891632
car_eval_4	TomekLinks	0.891536
car_eval_4	<i>None</i>	0.891306
car_eval_4	NeighbourhoodCleaningRule	0.885788
car_eval_4	EditedNearestNeighbours	0.874307
car_eval_4	RepeatedEditedNearestNeighbours	0.874307
car_eval_4	SMOTEENN	0.873877
car_eval_4	InstanceHardnessThreshold	0.871338
car_eval_4	RandomUnderSampler	0.724921
car_eval_4	NearMiss	0.398794

Continued on next page

Table 4 – *Continued from previous page*

Dataset	Method	AUPRC
coil_2000	InstanceHardnessThreshold	0.130768
coil_2000	RandomUnderSampler	0.127169
coil_2000	NeighbourhoodCleaningRule	0.124753
coil_2000	RepeatedEditedNearestNeighbours	0.124138
coil_2000	EditedNearestNeighbours	0.124020
coil_2000	TomekLinks	0.123720
coil_2000	OneSidedSelection	0.123490
coil_2000	AllKNN	0.123323
coil_2000	<i>None</i>	0.122316
coil_2000	CondensedNearestNeighbour	0.122222
coil_2000	SMOTEENN	0.121458
coil_2000	SVMSMOTE	0.120430
coil_2000	RandomOverSampler	0.119438
coil_2000	BorderlineSMOTE	0.118154
coil_2000	SMOTETomek	0.117747
coil_2000	ADASYN	0.117205
coil_2000	SMOTE	0.116818
coil_2000	SMOTEN	0.102871
coil_2000	NearMiss	0.070939
ecoli	OneSidedSelection	0.679323
ecoli	<i>None</i>	0.670092
ecoli	NeighbourhoodCleaningRule	0.669095
ecoli	TomekLinks	0.666434
ecoli	EditedNearestNeighbours	0.660769
ecoli	AllKNN	0.655290
ecoli	RandomUnderSampler	0.647470
ecoli	ADASYN	0.637569
ecoli	RandomOverSampler	0.627547
ecoli	SMOTE	0.626608
ecoli	SMOTETomek	0.622792
ecoli	SMOTEN	0.620329
ecoli	RepeatedEditedNearestNeighbours	0.617065
ecoli	SVMSMOTE	0.615822
ecoli	SMOTEENN	0.615135
ecoli	BorderlineSMOTE	0.613431
ecoli	CondensedNearestNeighbour	0.611176
ecoli	InstanceHardnessThreshold	0.530402
ecoli	NearMiss	0.279424
isolet	TomekLinks	0.856045
isolet	OneSidedSelection	0.855513
isolet	<i>None</i>	0.854120

Continued on next page

Table 4 – *Continued from previous page*

Dataset	Method	AUPRC
isolet	NeighbourhoodCleaningRule	0.850669
isolet	RandomOverSampler	0.846288
isolet	EditedNearestNeighbours	0.840449
isolet	SVMSMOTE	0.835170
isolet	AllKNN	0.834430
isolet	SMOTE	0.828889
isolet	SMOTETomek	0.828889
isolet	SMOTEN	0.824984
isolet	RepeatedEditedNearestNeighbours	0.822052
isolet	CondensedNearestNeighbour	0.820545
isolet	ADASYN	0.807127
isolet	BorderlineSMOTE	0.795150
isolet	RandomUnderSampler	0.776272
isolet	SMOTEENN	0.760503
isolet	InstanceHardnessThreshold	0.624215
isolet	NearMiss	0.387811
letter_img	ADASYN	0.934319
letter_img	NeighbourhoodCleaningRule	0.934012
letter_img	RepeatedEditedNearestNeighbours	0.933787
letter_img	EditedNearestNeighbours	0.932822
letter_img	<i>None</i>	0.932303
letter_img	RandomOverSampler	0.932142
letter_img	SVMSMOTE	0.931972
letter_img	TomekLinks	0.931817
letter_img	AllKNN	0.931713
letter_img	OneSidedSelection	0.931284
letter_img	SMOTE	0.928943
letter_img	SMOTETomek	0.928943
letter_img	BorderlineSMOTE	0.924850
letter_img	SMOTEENN	0.924516
letter_img	SMOTEN	0.922953
letter_img	InstanceHardnessThreshold	0.893851
letter_img	CondensedNearestNeighbour	0.877469
letter_img	RandomUnderSampler	0.805643
letter_img	NearMiss	0.623239
libras_move	BorderlineSMOTE	0.896869
libras_move	SVMSMOTE	0.881083
libras_move	RandomOverSampler	0.880520
libras_move	ADASYN	0.870014
libras_move	SMOTE	0.850161
libras_move	SMOTETomek	0.850161

Continued on next page

Table 4 – *Continued from previous page*

Dataset	Method	AUPRC
libras_move	EditedNearestNeighbours	0.849418
libras_move	NeighbourhoodCleaningRule	0.848337
libras_move	OneSidedSelection	0.845898
libras_move	<i>None</i>	0.834689
libras_move	TomekLinks	0.834689
libras_move	AllKNN	0.833356
libras_move	RepeatedEditedNearestNeighbours	0.831513
libras_move	SMOTEENN	0.824668
libras_move	SMOTEN	0.797956
libras_move	InstanceHardnessThreshold	0.719700
libras_move	CondensedNearestNeighbour	0.666148
libras_move	RandomUnderSampler	0.665363
libras_move	NearMiss	0.517403
mammography	SVMSMOTE	0.632852
mammography	TomekLinks	0.624105
mammography	RandomOverSampler	0.618372
mammography	<i>None</i>	0.616847
mammography	SMOTE	0.606156
mammography	SMOTETomek	0.605682
mammography	NeighbourhoodCleaningRule	0.603693
mammography	CondensedNearestNeighbour	0.596846
mammography	EditedNearestNeighbours	0.593231
mammography	BorderlineSMOTE	0.592917
mammography	AllKNN	0.580091
mammography	OneSidedSelection	0.576425
mammography	RepeatedEditedNearestNeighbours	0.566129
mammography	SMOTEENN	0.563037
mammography	ADASYN	0.549686
mammography	RandomUnderSampler	0.510061
mammography	SMOTEN	0.503070
mammography	InstanceHardnessThreshold	0.305018
mammography	NearMiss	0.038770
oil	BorderlineSMOTE	0.484308
oil	SMOTE	0.482234
oil	ADASYN	0.480444
oil	SMOTETomek	0.480316
oil	SVMSMOTE	0.477834
oil	<i>None</i>	0.438855
oil	NeighbourhoodCleaningRule	0.437105
oil	SMOTEN	0.432911
oil	TomekLinks	0.430262

Continued on next page

Table 4 – *Continued from previous page*

Dataset	Method	AUPRC
oil	RandomOverSampler	0.429126
oil	OneSidedSelection	0.428500
oil	EditedNearestNeighbours	0.427453
oil	SMOTEENN	0.421939
oil	AlkNN	0.396827
oil	RepeatedEditedNearestNeighbours	0.374801
oil	InstanceHardnessThreshold	0.318653
oil	CondensedNearestNeighbour	0.308418
oil	RandomUnderSampler	0.300908
oil	NearMiss	0.202147
optical_digits	AllKNN	0.946737
optical_digits	EditedNearestNeighbours	0.946591
optical_digits	<i>None</i>	0.946543
optical_digits	NeighbourhoodCleaningRule	0.945674
optical_digits	TomekLinks	0.944721
optical_digits	RepeatedEditedNearestNeighbours	0.944429
optical_digits	OneSidedSelection	0.938495
optical_digits	SMOTE	0.938098
optical_digits	SMOTETomek	0.938098
optical_digits	RandomOverSampler	0.937414
optical_digits	SMOTEENN	0.935060
optical_digits	SVMSMOTE	0.930706
optical_digits	SMOTEN	0.929500
optical_digits	BorderlineSMOTE	0.923988
optical_digits	ADASYN	0.923797
optical_digits	RandomUnderSampler	0.890297
optical_digits	CondensedNearestNeighbour	0.849241
optical_digits	InstanceHardnessThreshold	0.842486
optical_digits	NearMiss	0.701474
ozone_level	InstanceHardnessThreshold	0.221960
ozone_level	RepeatedEditedNearestNeighbours	0.198115
ozone_level	<i>None</i>	0.197729
ozone_level	EditedNearestNeighbours	0.196054
ozone_level	OneSidedSelection	0.195971
ozone_level	NeighbourhoodCleaningRule	0.195696
ozone_level	AlkNN	0.194429
ozone_level	RandomOverSampler	0.194208
ozone_level	BorderlineSMOTE	0.194146
ozone_level	SVMSMOTE	0.194020
ozone_level	TomekLinks	0.192708
ozone_level	SMOTEENN	0.186460

Continued on next page

Table 4 – *Continued from previous page*

Dataset	Method	AUPRC
ozone_level	SMOTETomek	0.184983
ozone_level	CondensedNearestNeighbour	0.184195
ozone_level	RandomUnderSampler	0.182302
ozone_level	ADASYN	0.177766
ozone_level	SMOTE	0.176374
ozone_level	SMOTEN	0.157684
ozone_level	NearMiss	0.036128
pen_digits	RandomOverSampler	0.960806
pen_digits	TomekLinks	0.960350
pen_digits	RepeatedEditedNearestNeighbours	0.960302
pen_digits	<i>None</i>	0.960292
pen_digits	EditedNearestNeighbours	0.959954
pen_digits	NeighbourhoodCleaningRule	0.959947
pen_digits	OneSidedSelection	0.959765
pen_digits	AllKNN	0.959450
pen_digits	SMOTE	0.957603
pen_digits	SMOTETomek	0.957603
pen_digits	SMOTEENN	0.956401
pen_digits	SMOTEN	0.951931
pen_digits	InstanceHardnessThreshold	0.923645
pen_digits	SVMSMOTE	0.922007
pen_digits	RandomUnderSampler	0.921658
pen_digits	ADASYN	0.916603
pen_digits	BorderlineSMOTE	0.908667
pen_digits	CondensedNearestNeighbour	0.868471
pen_digits	NearMiss	0.675025
protein_homo	AllKNN	0.839470
protein_homo	EditedNearestNeighbours	0.838064
protein_homo	NeighbourhoodCleaningRule	0.835545
protein_homo	OneSidedSelection	0.834851
protein_homo	RepeatedEditedNearestNeighbours	0.834632
protein_homo	TomekLinks	0.832761
protein_homo	<i>None</i>	0.830796
protein_homo	RandomOverSampler	0.818520
protein_homo	SMOTEN	0.809633
protein_homo	InstanceHardnessThreshold	0.788383
protein_homo	SVMSMOTE	0.769511
protein_homo	CondensedNearestNeighbour	0.763495
protein_homo	BorderlineSMOTE	0.759034
protein_homo	SMOTETomek	0.719719
protein_homo	SMOTE	0.719372

Continued on next page

Table 4 – *Continued from previous page*

Dataset	Method	AUPRC
protein_homo	ADASYN	0.716366
protein_homo	SMOTEENN	0.715738
protein_homo	RandomUnderSampler	0.683711
protein_homo	NearMiss	0.137922
satimage	<i>None</i>	0.581587
satimage	OneSidedSelection	0.580241
satimage	TomekLinks	0.578822
satimage	NeighbourhoodCleaningRule	0.575820
satimage	RandomOverSampler	0.566923
satimage	SMOTE	0.563886
satimage	SMOTETomek	0.563886
satimage	EditedNearestNeighbours	0.563377
satimage	SVMSMOTE	0.560030
satimage	CondensedNearestNeighbour	0.553217
satimage	SMOTEN	0.552696
satimage	AllKNN	0.552265
satimage	ADASYN	0.543886
satimage	BorderlineSMOTE	0.535283
satimage	SMOTEENN	0.525733
satimage	RepeatedEditedNearestNeighbours	0.525305
satimage	RandomUnderSampler	0.513260
satimage	InstanceHardnessThreshold	0.410938
satimage	NearMiss	0.121733
scene	AllKNN	0.260258
scene	EditedNearestNeighbours	0.255101
scene	SVMSMOTE	0.254637
scene	NeighbourhoodCleaningRule	0.248582
scene	OneSidedSelection	0.248209
scene	RepeatedEditedNearestNeighbours	0.246716
scene	TomekLinks	0.241893
scene	<i>None</i>	0.240611
scene	BorderlineSMOTE	0.238879
scene	RandomOverSampler	0.236289
scene	ADASYN	0.233983
scene	SMOTE	0.231977
scene	SMOTETomek	0.231817
scene	RandomUnderSampler	0.229056
scene	SMOTEENN	0.227890
scene	SMOTEN	0.224181
scene	CondensedNearestNeighbour	0.216484
scene	InstanceHardnessThreshold	0.200717

Continued on next page

Table 4 – *Continued from previous page*

Dataset	Method	AUPRC
scene	NearMiss	0.102695
sick_euthyroid	SVMSMOTE	0.785684
sick_euthyroid	SMOTETomek	0.784999
sick_euthyroid	RandomOverSampler	0.784531
sick_euthyroid	SMOTE	0.782663
sick_euthyroid	BorderlineSMOTE	0.782143
sick_euthyroid	<i>None</i>	0.780421
sick_euthyroid	ADASYN	0.779566
sick_euthyroid	TomekLinks	0.778363
sick_euthyroid	NeighbourhoodCleaningRule	0.777484
sick_euthyroid	OneSidedSelection	0.775670
sick_euthyroid	EditedNearestNeighbours	0.775141
sick_euthyroid	SMOTEN	0.770853
sick_euthyroid	AllKNN	0.765810
sick_euthyroid	RepeatedEditedNearestNeighbours	0.763223
sick_euthyroid	SMOTEENN	0.759671
sick_euthyroid	CondensedNearestNeighbour	0.733857
sick_euthyroid	RandomUnderSampler	0.696834
sick_euthyroid	InstanceHardnessThreshold	0.676978
sick_euthyroid	NearMiss	0.398005
solar_flare_m0	CondensedNearestNeighbour	0.160947
solar_flare_m0	NeighbourhoodCleaningRule	0.156081
solar_flare_m0	AllKNN	0.155723
solar_flare_m0	SMOTEENN	0.154573
solar_flare_m0	RepeatedEditedNearestNeighbours	0.151498
solar_flare_m0	EditedNearestNeighbours	0.149907
solar_flare_m0	TomekLinks	0.149051
solar_flare_m0	RandomUnderSampler	0.147578
solar_flare_m0	InstanceHardnessThreshold	0.146633
solar_flare_m0	OneSidedSelection	0.144293
solar_flare_m0	SVMSMOTE	0.142220
solar_flare_m0	RandomOverSampler	0.141912
solar_flare_m0	<i>None</i>	0.141722
solar_flare_m0	BorderlineSMOTE	0.139522
solar_flare_m0	SMOTEN	0.138550
solar_flare_m0	SMOTE	0.137186
solar_flare_m0	SMOTETomek	0.137186
solar_flare_m0	ADASYN	0.129831
solar_flare_m0	NearMiss	0.100430
spectrometer	SMOTEN	0.767142
spectrometer	EditedNearestNeighbours	0.766650

Continued on next page

Table 4 – *Continued from previous page*

Dataset	Method	AUPRC
spectrometer	RepeatedEditedNearestNeighbours	0.766299
spectrometer	<i>None</i>	0.765167
spectrometer	AllKNN	0.765159
spectrometer	SVMSMOTE	0.761152
spectrometer	TomekLinks	0.759670
spectrometer	BorderlineSMOTE	0.759096
spectrometer	NeighbourhoodCleaningRule	0.758629
spectrometer	SMOTETomek	0.750427
spectrometer	SMOTE	0.747447
spectrometer	ADASYN	0.740255
spectrometer	RandomOverSampler	0.739555
spectrometer	SMOTEENN	0.737696
spectrometer	OneSidedSelection	0.731471
spectrometer	InstanceHardnessThreshold	0.703745
spectrometer	RandomUnderSampler	0.698745
spectrometer	CondensedNearestNeighbour	0.647825
spectrometer	NearMiss	0.393815
thyroid_sick	<i>None</i>	0.768265
thyroid_sick	TomekLinks	0.767235
thyroid_sick	OneSidedSelection	0.766953
thyroid_sick	RandomOverSampler	0.766101
thyroid_sick	NeighbourhoodCleaningRule	0.766076
thyroid_sick	ADASYN	0.761758
thyroid_sick	SMOTETomek	0.758488
thyroid_sick	SMOTE	0.756963
thyroid_sick	AllKNN	0.756619
thyroid_sick	SVMSMOTE	0.755433
thyroid_sick	EditedNearestNeighbours	0.753655
thyroid_sick	BorderlineSMOTE	0.749557
thyroid_sick	RepeatedEditedNearestNeighbours	0.745291
thyroid_sick	CondensedNearestNeighbour	0.732923
thyroid_sick	SMOTEENN	0.726312
thyroid_sick	SMOTEN	0.721404
thyroid_sick	RandomUnderSampler	0.658317
thyroid_sick	InstanceHardnessThreshold	0.646062
thyroid_sick	NearMiss	0.450881
us_crime	SMOTEN	0.460008
us_crime	NeighbourhoodCleaningRule	0.457170
us_crime	TomekLinks	0.452950
us_crime	OneSidedSelection	0.451024
us_crime	RepeatedEditedNearestNeighbours	0.450062

Continued on next page

Table 4 – *Continued from previous page*

Dataset	Method	AUPRC
us_crime	SVMSMOTE	0.448927
us_crime	<i>None</i>	0.448593
us_crime	AllKNN	0.448385
us_crime	EditedNearestNeighbours	0.445048
us_crime	CondensedNearestNeighbour	0.431910
us_crime	RandomUnderSampler	0.429545
us_crime	RandomOverSampler	0.429413
us_crime	SMOTE	0.420780
us_crime	SMOTETomek	0.420780
us_crime	BorderlineSMOTE	0.416748
us_crime	SMOTEENN	0.409801
us_crime	ADASYN	0.403203
us_crime	InstanceHardnessThreshold	0.391133
us_crime	NearMiss	0.310530
webpage	OneSidedSelection	0.716597
webpage	TomekLinks	0.716552
webpage	<i>None</i>	0.715568
webpage	CondensedNearestNeighbour	0.709512
webpage	NeighbourhoodCleaningRule	0.694978
webpage	EditedNearestNeighbours	0.685888
webpage	AllKNN	0.676386
webpage	RandomOverSampler	0.666281
webpage	RepeatedEditedNearestNeighbours	0.661258
webpage	SVMSMOTE	0.645779
webpage	SMOTE	0.628776
webpage	SMOTETomek	0.628776
webpage	SMOTEN	0.608370
webpage	BorderlineSMOTE	0.593482
webpage	ADASYN	0.579732
webpage	SMOTEENN	0.549320
webpage	RandomUnderSampler	0.511892
webpage	InstanceHardnessThreshold	0.508713
webpage	NearMiss	0.211698
wine_quality	RandomOverSampler	0.287078
wine_quality	<i>None</i>	0.283333
wine_quality	SVMSMOTE	0.275223
wine_quality	TomekLinks	0.274099
wine_quality	NeighbourhoodCleaningRule	0.273313
wine_quality	OneSidedSelection	0.271907
wine_quality	AllKNN	0.270325
wine_quality	EditedNearestNeighbours	0.268315

Continued on next page

Table 4 – *Continued from previous page*

Dataset	Method	AUPRC
wine_quality	BorderlineSMOTE	0.268253
wine_quality	RepeatedEditedNearestNeighbours	0.263043
wine_quality	SMOTETomek	0.260419
wine_quality	SMOTE	0.258939
wine_quality	ADASYN	0.252852
wine_quality	CondensedNearestNeighbour	0.239557
wine_quality	SMOTEENN	0.231595
wine_quality	SMOTEN	0.230773
wine_quality	InstanceHardnessThreshold	0.229103
wine_quality	RandomUnderSampler	0.206871
wine_quality	NearMiss	0.057979
yeast_me2	NeighbourhoodCleaningRule	0.367299
yeast_me2	EditedNearestNeighbours	0.366031
yeast_me2	SVMSMOTE	0.364783
yeast_me2	BorderlineSMOTE	0.356850
yeast_me2	RepeatedEditedNearestNeighbours	0.356482
yeast_me2	AllKNN	0.356166
yeast_me2	OneSidedSelection	0.352041
yeast_me2	TomekLinks	0.350277
yeast_me2	SMOTE	0.347099
yeast_me2	<i>None</i>	0.342411
yeast_me2	SMOTETomek	0.342317
yeast_me2	ADASYN	0.339819
yeast_me2	SMOTEENN	0.309819
yeast_me2	RandomOverSampler	0.309086
yeast_me2	CondensedNearestNeighbour	0.307005
yeast_me2	InstanceHardnessThreshold	0.289938
yeast_me2	RandomUnderSampler	0.265066
yeast_me2	SMOTEN	0.234466
yeast_me2	NearMiss	0.113107
yeast_ml8	InstanceHardnessThreshold	0.120360
yeast_ml8	RandomUnderSampler	0.108407
yeast_ml8	TomekLinks	0.108024
yeast_ml8	RepeatedEditedNearestNeighbours	0.106284
yeast_ml8	OneSidedSelection	0.105521
yeast_ml8	SMOTEENN	0.104856
yeast_ml8	SVMSMOTE	0.104654
yeast_ml8	BorderlineSMOTE	0.104453
yeast_ml8	AllKNN	0.104293
yeast_ml8	RandomOverSampler	0.104158
yeast_ml8	EditedNearestNeighbours	0.103038

Continued on next page

Table 4 – *Continued from previous page*

Dataset	Method	AUPRC
yeast_ml8	<i>None</i>	0.101586
yeast_ml8	SMOTEN	0.100680
yeast_ml8	NeighbourhoodCleaningRule	0.099834
yeast_ml8	ADASYN	0.098387
yeast_ml8	SMOTE	0.097896
yeast_ml8	SMOTETomek	0.097896
yeast_ml8	NearMiss	0.093707
yeast_ml8	CondensedNearestNeighbour	0.088049

E Dataset Coverage

To avoid ambiguity between canonical dataset families and benchmark-specific variants, we list the exact 27 dataset identifiers used in the performance tables.

Table 5: Dataset identifiers used in the benchmark (27 total).

Dataset ID
abalone, abalone_19, arrhythmia, car_eval_34, car_eval_4, coil_2000, ecoli, isolet, letter_img, libras_move, mammography, oil, optical_digits, ozone_level, pen_digits, protein_homo, satimage, scene, sick_euthyroid, solar_flare_m0, spectrometer, thyroid_sick, us_crime, webpage, wine_quality, yeast_me2, yeast_ml8.